Acoustic and relaxation processes in supercooled orthoterphenyl by optical-heterodyne transient grating experiment

R. Torre,[1,2] A. Taschin,[1,3] and M. Sampoli[1,4]
[1]*INFM, Unità di Firenze, largo Enrico Fermi 2, I-50125, Firenze, Italy*
[2]*LENS, Università di Firenze, largo Enrico Fermi 2, I-50125, Firenze, Italy*
[3]*Dip. di Fisica, Università di Firenze, largo Enrico Fermi 2, I-50125, Firenze, Italy*
[4]*Dip. di Energetica, Università di Firenze, via S. Marta, Firenze, Italy*
(Received 29 June 2001; published 20 November 2001)

The dynamics of the fragile glass-forming orthoterphenyl have been investigated by transient grating experiments with an heterodyne detection technique. We measured the relaxation processes of this glass former over more than six decades in time with an excellent signal-to-noise ratio. Acoustic, structural, and thermal relaxations have been clearly identified in a time-frequency window not covered by previous spectroscopic studies and their characteristic dynamic parameters have been measured as a function of temperature and wave vector. A detailed comparison with the density response function, calculated on the basis of generalized hydrodynamic model, has been worked out.

DOI: 10.1103/PhysRevE.64.061504 PACS number(s): 64.70.Pf, 78.47.+p

I. INTRODUCTION

Supercooled liquids and glasses have been the subject, during the last years, of an extensive theoretical and experimental study [1,2]. One of most important features of these materials is the wide range of time scales over which relaxations occurs. The relaxation times span over many decades (up to 13 decades) when temperature is varied from the melting to glass transition temperature. Indeed, these relaxation processes have a complex nature that, despite the recent research efforts, remain unclear in many aspects. Among others, a fundamental issue is the interplay of different dynamical variables present in these materials, so that rotational dynamics and its coupling with the translational variables are under an intense experimental investigation [3–5]. Even when a single dynamic variable (e.g., density) is studied, many processes are involved in glass dynamics (for example, the acoustic, structural, and thermal relaxations) and they are usually characterized by different time scales. From the experimental point of view, it is of fundamental importance to measure the investigated variables over the full temporal (or frequency) range. This is hardly accomplished by the combination of several spectroscopic techniques (e.g., light-scattering, photon correlation spectroscopy, etc.) since the very wide time (or frequency) domain cannot be fully investigated, and this often preserves a reliable analysis of the data.

The transient grating techniques (TG) give a unique experimental insight in to the dynamics of fluids and glassy materials [6]. Recently, this technique has been applied to the study of dynamics of supercooled liquids [7]. Using a continuous wave (CW) beam probe it has been possible to investigate a very wide temporal range, from nanoseconds to milliseconds, in a single experiment. Indeed, this is a unique experimental access to glass dynamics.

In this paper, we present a study of relaxation dynamics of the fragile glass-former ortho-terphenyl (OTP) by optical heterodyne detected transient grating (HD-TG) experiment. Acoustic, thermal, and structural relaxations are investigated at different wave vectors and in a wide temperature range, from above the melting down to the glass transition. This HD-TG experiment produces data with an extremely high signal-to-noise ratio and it allows us to detect and measure very weak signals. We present a study of the density dynamics, and of its complex relaxation pattern, in a prototype of the fragile glass formers, OTP. Furthermore, we show some features of the slow thermal relaxation that the standard hydrodynamic model cannot explain properly.

The paper begins (Sec. II) with a brief description of the transient grating experiment and in particular we underline the improvements achieved by using an optical heterodyne detection. In Sec. III, the theoretical background, needed for the data analysis and interpretation, is given. A detailed description of the OTP measurements is written in Sec. IV and in Sec. V, we present all data and their analysis. Section VI is devoted to discussions and conclusions.

II. HETERODYNE TRANSIENT GRATING EXPERIMENT

In a transient grating (TG) experiment, two high-power laser pulses, obtained by dividing a single pulsed laser beam, interfere inside the sample and they produce a spatially periodic variation of the index of refraction [6,8]. A second laser beam, typically of a different wavelength, is acting as a probe. It impinges on the induced grating at the Bragg angle and it produces a diffracted beam, spatially separated by the pump pulses and probe beam itself, see Fig. 1. This diffracted beam is the signal measured in a TG experiments and it yields the dynamic information from the relaxing TG. The spatial modulation of the grating defines a wave-vector q

$$q = \frac{4\pi \sin\left(\frac{\theta_e}{2}\right)}{\lambda_e}, \tag{1}$$

where λ_e and θ_e are the wavelength and the incidence angle of the excitation laser pulses. When, as usual, the homodyne

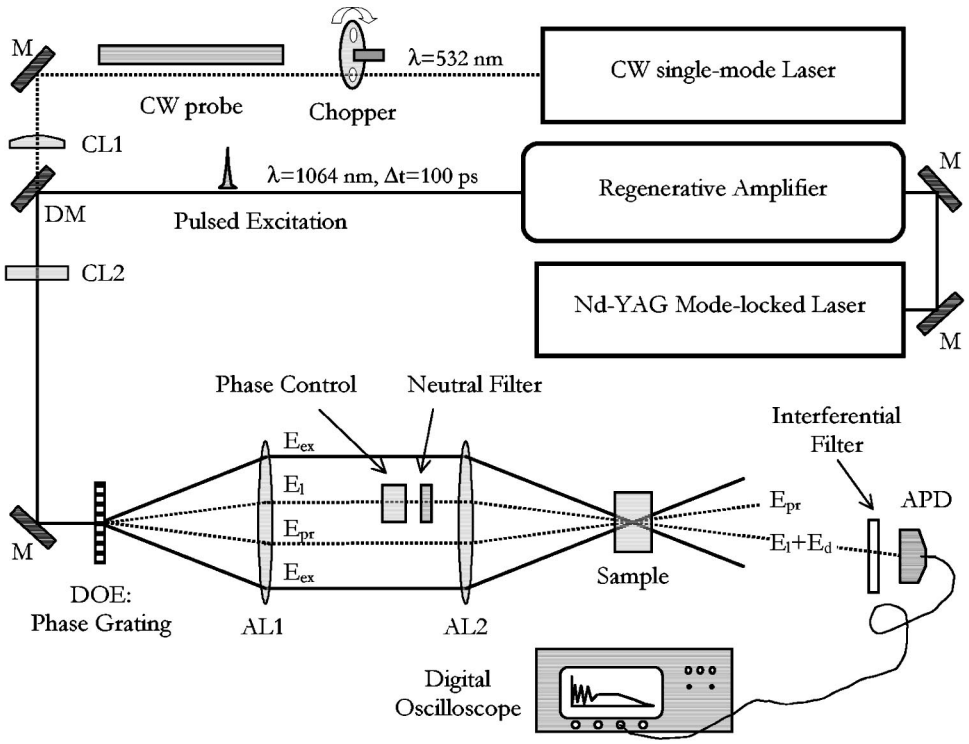

FIG. 1. Optical setup and laser system for HD-TG experiment with optical heterodyne detection: M: mirror; CL#: cylindrical lens; DM: dicroic mirror; DOE: diffractive optic element; AL#: achromatic lens; APD: avalanche photodiode.

scheme is used to detect the diffracted beam, the diffraction efficiency is proportional to the square of the refraction index variation, so that small variations produce even smaller signals. A considerable improvement may be obtained by using an optical heterodyne detection (HD). In a HD-TG experiment, the measured signal is

$$S(q,t) \propto \langle |E_d(q,t)|^2 \rangle + \langle |E_l|^2 \rangle + 2\langle |E_d(q,t)| \rangle \langle |E_l| \rangle \cos \Delta\varphi, \tag{2}$$

where E_d is the electric field diffracted by the TG, E_l is the local beating field, and $\Delta\varphi$ is the phase difference between the E_d and E_l, (see Fig. 1). $\langle \cdot \rangle$ represent the time averaging over the optical period. The three terms in the right-hand side (r.h.s.) of Eq. 2, are the homodyne ($\langle |E_d|^2 \rangle$), the local field ($\langle |E_l|^2 \rangle$), and the heterodyne contributions ($2\langle |E_d(q,t)| \rangle \times \langle |E_l| \rangle \cos \Delta\varphi$). If the local field has a constant and high intensity (higher than the diffracted one), the homodyne contribution becomes negligible and the time variation of the signal is dominated by the heterodyne term. Indeed, this last term may be experimentally isolated subtracting two signals characterized by different phases. Recording a first signal, S_+, with $\Delta\varphi_+ = 2n\pi$ and then a second one, S_-, with $\Delta\varphi_- = (2n+1)\pi$ (n integer), it is evident that

$$S_{HD}(q,t) = [S_+ - S_-] \propto \langle |E_d(q,t)| \rangle \langle |E_l| \rangle. \tag{3}$$

There are two major advantages in using the heterodyne instead of the homodyne detection. First, it improves substantially the signal-to-noise ratio in the all-time window, both because of the signal increment and because of the discharge of all the spurious signals that are not phase sensitive. Second, it enhances enormously the sensitivity since the recorded signal is directly proportional to $\langle |E_d| \rangle$ instead of being proportional to its square. In the study of materials with a weak-scattering efficiency and complex responses, these features turn out to be of basic importance. Furthermore, the HD allows us to measure the very long-time relaxation times, where the TG signals become very weak for any materials. Nevertheless, the effective realization of such detection is quite difficult at optical frequencies. Indeed, to get an interferometric phase stability between the diffracted and the local field is not a simple experimental task, and so, only a few HD-TG experiments have been realized up to now [6]. Recently, the introduction of phase gratings in the optical setup of TG experiments has reduced considerably the difficulties of using a heterodyne detection [9,10]. The details of this new setup will be described in Sec. IV A.

Formally, in the limit of linear response theory, the average diffracted field is proportional to the material response function convoluted with the excitation force produced by the laser excitation [8]. Assuming the impulsive limit in time (i.e., the excitation time much shorter than the observable characteristic times) and in wave vector (i.e., the excitation spot size much larger than the material wavelength scale) we have

$$S_{HD}(q,t) \propto \langle |E_d(q,t)| \rangle \propto R(q,t). \tag{4}$$

The response function, $R(q,t)$, describes how the exciting pulses are effective in producing a TG, i.e., a periodic variation of the optical properties out of equilibrium, and how this variation is relaxing toward equilibrium. If the duration of exciting pulses has to be taken into account, i.e., if some characteristic times in the response cannot be considered long enough with respect to the pulse duration, the total response has to be calculated from the appropriate convolution.

The response function has a tensorial nature R_{ijkl} where the different components are selected through the excitation,

probing, and detection directions of polarizations. In the present experiment, all these polarizations are taken vertical, i.e., normal to the scattering plane, (see Sec. IV A for details) and then we are dealing with a single tensorial component of the response function, R_{VVVV}.

The interaction of the excitation laser field with the material is responsible for generating the TG and it defines the appropriate response function. Depending on the nature of this interaction, the excitation laser pulses may produce a modulation in the real part of the refraction index (i.e., a birefringence and/or a phase grating), and/or a modulation in the imaginary part of it (i.e., a dichroic and/or absorption grating). Which grating is excited and how its dynamics reflects the material properties is a complex problem that may be solved only under certain conditions and approximations.

As well as other molecules of glass-forming materials investigated by TG [7], our OTP molecule has no electronic absorption band at the pump and probe wavelengths. However, the strong near-infrared pulses are absorbed weakly by overtones and/or combinations of vibrational bands. Typically, these vibrational excitations thermalize in a few picoseconds. According to Yang and Nelson and Paolucci and Nelson [7], the induced TG may be described approximately as a pure phase grating generated by two different mechanisms of laser-matter interaction: a temperature grating produced by the field-induced heating and a pressure electrostrictive grating due to the field gradient. In this approach, no birefringence effects are taken into account, such as a modification of the molecular polarizability orientations due to the field effect (optical Kerr effect) or to a molecular alignment induced by the roto-translation coupling. Indeed, the birefrengence effects should be weak in materials composed of molecules of nearly isotropic shape and without strong anisotropic interactions. For these materials, the total response should be considered mainly driven by the density. In the case of OTP, under the present investigation, we verified experimentally this hypothesis measuring the S_{HHVV} signal (with the probe and detection polarizations, HH, perpendicular to the excitation one, VV) and comparing that with the S_{VVVV} signal: no meaningful difference has been detected for any temperature. So, in OTP, no relevant birefringence effects are present and the response function is characterized by the density dynamics. Vice versa, a strong difference has been detected in other glass formers, (e.g., *m* toluidine and salol), showing that the response function of glass formers made of anisotropic molecules must include birefringence and roto-translational coupling effects [4].

The measured response function is proportional to the q component of the induced density variations and it may be described, according to a simple physical model, through three different contributions. Two of them are the response to the heating effect and one to the electrostriction effect. (i) The first contribution is substantially a ''fast-liquid'' response to the sudden heating in the sample: the temperature grating launches a sound wave of frequency $\omega_A = c_A q$ that is damped with an acoustic time constant τ_A and then the local temperature relaxes due to the thermal diffusivity with a time constant τ_H. Therefore, this contribution may be written as $\rho_q^{(h,s)} \propto [1-\exp(-t/\tau_A)\cos(\omega_A t)]\exp(-t/\tau_H)$. (ii) The second contribution is a ''viscous-liquid'' response to the heat flux. This is characterized by a slow density variation that grows up with a time constant τ_R and vanishes again with the thermal diffusivity constant, so the corresponding density variation is $\rho_q^{(h,r)} \propto [1-\exp(-t/\tau_R)]\exp(-t/\tau_H)$. (iii) The sudden variation of the density momentum, due to the electrostriction effects, again launches a sound wave of the same frequency $\omega_A = c_A q$ around the normal density that is damped always with the same acoustic time constant, so the last contribution is $\rho_q^{(e)} \propto \exp(-t/\tau_A)\sin(\omega_A t)$.

Intuitively, the sum of these contributions will be the measured signal. Obviously, there are interactions among these contributions when the time constants have similar values. Further, the viscous-liquid response in a supercooled liquid is characterized by a distribution of relaxation times and it cannot be described by a single relaxation. Nevertheless, this very simple and intuitive model contains already many of the physical information present in the density response. In the next section, we will summarize a formal derivation of the density response function from the hydrodynamic equations and the important relations among the parameters we have introduced.

III. THEORETICAL BACKGROUND

The generalized hydrodynamics equations have been used to describe the frequency resolved light-scattering experiments [11]. These equations express the conservation laws present in the dynamics of the fluid: the conservation of mass, momentum, and energy. The continuity, Navier-Stokes and energy equations, when we neglect the rotational effects, we use the linearized form (small fluctuation out of equilibrium) and we apply the Fourier-Laplace transform (FLT), are [12]

$$s\widetilde{\delta\rho}_q(s) + iq\tilde{J}_{q\parallel}(s) = \delta\rho_q(0),$$

$$[s+\phi_L(s)q^2]\tilde{J}_{q\parallel}(s) + i(qc_o^2/\gamma)[\widetilde{\delta\rho}_q(s) + \alpha\rho_o\widetilde{\delta T}_q(s)] = J_{q\parallel}(0),$$

$$(s+\gamma\chi q^2)\rho_o\widetilde{\delta T}_q(s) + i[q(\gamma-1)/\alpha]\tilde{J}_{q\parallel}(s)\,\delta\rho_q(s) + iqJ_{q\parallel}(s) = \rho_o\delta T_q(0),$$

where $\widetilde{\delta x}_q(s)$ stands for the FLT of the fluctuating quantity $\delta x(\mathbf{r},t)$, i.e.,

$$\widetilde{\delta x}_q(s) = \int_0^\infty dt\,\exp(-st)\,\delta x_q(t) = \int_0^\infty dt\,\exp(-st)\int_{-\infty}^{+\infty} d^3r\,\exp(i\mathbf{q}\cdot\mathbf{r})\,\delta x(\mathbf{r},t),$$

and ρ_o is the equilibrium mass density, $J_{q\parallel}$ the component parallel to $\mathbf{q}$ of the mass current density, δT_q the fluctuating temperature, c_o the adiabatic zero-frequency sound velocity, $\gamma = C_p/C_v$ the ratio of the specific heats, $\alpha =$

$-(\partial\rho/\partial T)_p/\rho$ the coefficient of thermal expansion, $\chi = k(\rho_o C_p)^{-1}$ the thermal diffusivity, and $\rho_o \phi_L$ the longitudinal kinematic viscosity.

Following Yang and Nelson, Paolucci and Nelson, and Yang and Nelson [7,13], we can solve formally the previous equations with the starting conditions $\delta\rho_q(0)=0$, $J_{q\|}(0) = i\,q\,F$, and $\rho_o \delta T_q(0) = Q/C_v$ and we obtain that the HD signal may be written, in Nelson's notation, as

$$S_{HD}(q,t) \propto R_\rho(q,t) = -FG_{\rho\rho}(q,t) + QG_{\rho T}(q,t), \quad (5)$$

where $G_{\rho\rho}(q,t)$ is the response to the electrostriction (also called impulsive stimulated brillouin scattering, ISBS), and $G_{\rho T}(q,t)$ to the absorption (also called impulsive stimulated thermal scattering, ISTS) [6,7]. F and Q are two constants that define, respectively, the magnitude of the electrostriction and heating effects in the limit of infinitely short pump-laser pulses.

In order to calculate the density response function from the hydrodynamic equations, we have to know all the coefficients, and in particular, the time (or frequency) dependence of the kinematic viscosity ϕ_L. Only for particular ϕ_L, is it possible to obtain analytical expressions for $G_{\rho\rho}(q,t)$ and $G_{\rho T}(q,t)$. One of them is the kinematic viscosity introduced by the Debye model of a viscous fluid [12]. Here, ϕ_L (or memory function for the elastic modulus) is approximated by the sum of two terms: $\phi_L(q,t) = v_L \delta(t) + (c_\infty^2 - c_0^2)\exp(-t/\tau_R)$. If we use this expression for ϕ_L and we suppose all the characteristic relaxation times are well separated from each other (i.e., the period of the acoustic wave, its damping time constant, the structural relaxation time, and the thermal diffusion time constant) the hydrodynamic equations give the following response functions [7,13,14]:

$$G_{\rho T}(q,t) \simeq A[e^{-\Gamma_H t} - e^{-\Gamma_A t}\cos(\omega_A t)] + B[e^{-\Gamma_H t} - e^{-t/\tau_R'}], \quad (6)$$

$$G_{\rho\rho}(q,t) \simeq C[e^{-\Gamma_A t}\sin(\omega_A t)], \quad (7)$$

where, Γ_H is the thermal damping rate ($\Gamma_H = 1/\tau_H = \chi q^2$), τ_R' the effective structural relaxation time [$\tau_R' = (c_A/c_0)^2 \tau_R$ being c_A the sound velocity], ω_A and $\Gamma_A = 1/\tau_A$ are the frequency and damping of acoustic longitudinal phonon, A, B, and C are constants dependent on sample and experimental setup. These response functions allow us to extract much information and to make expectations on the general behavior of the various parameters versus q and temperature. In particular, they predict a maximum on the acoustic damping both versus q and T, and a gradual shift of the sound velocity from c_0 to c_∞, lowering the temperature or increasing q. In fact, the following expressions hold [13]:

$$\omega_A = c_A q = [c_0 \sqrt{D + \sqrt{D^2 + (c_0 q \tau_R)^{-2}}}]q;$$

$$D = [c_\infty^2/c_0^2 - (c_0 q \tau_R)^{-2}]/2, \quad (8)$$

$$\frac{\Gamma_A}{q^2} = \frac{1}{2}\left\{[v_L + \chi(\gamma - c_0^2/c_\infty^2)] + \frac{c_\infty^2 - c_0^2}{1 + \omega_A^2 \tau_R^2}\right\}. \quad (9)$$

Further, when the condition $\omega_A \gg \Gamma_A \gg \tau_R^{-1} \gg \Gamma_H$ plus some other minor approximations are valid, the Debye-Waller factor or nonergodicity parameter $f_{q\to 0}(T)$ may be obtained from A and B coefficients, see Eq. 6, according to the following expression [13]:

$$f_{q\to 0}(T) = 1 - \frac{c_0^2}{c_\infty^2} = \frac{B}{A+B}. \quad (10)$$

However, the Debye model has some severe limitations. The structural relaxation close to the critical temperature cannot be reproduced by a single relaxation time but by a distribution of them; as it has been pointed out in many experimental works. As a consequence, more complex expressions for the kinematic viscosity have to be used, e.g., by a multiexponential distribution of relaxation times or by a stretched exponential approach [1]. When all the relaxation times of the actual distribution are separated from the other characteristic times, the kinematic viscosity affects only the second part of Eq. 6 and a complex relaxation may be put directly in the response as a stretched exponential, i.e., a Kohlrausch-Williams-Watts function [13]

$$G_{\rho T}(q,t) \simeq A[e^{-\Gamma_H t} - e^{-\Gamma_A t}\cos(\omega_A t)] + B[e^{-\Gamma_H t} - e^{-(t/\tau_S)^\beta}], \quad (11)$$

where the "relaxation-time" τ_S and the stretching factor β are fitting parameters for the relaxation-time distribution. This approximation has the advantage to keep an easy and readable form for the response function but it prevents the account for possible interactions among the different relaxing mechanisms. To compare τ_S with the relaxation times derived by other relaxation function (such as, for example, the Cole-Davidson function typically used in the analysis of the frequency domain data), the mean of the time distribution is calculated as $\langle \tau_S \rangle = \beta^{-1}\Gamma(\beta^{-1})\tau_S$.

We want to remark that the presence of a stretched exponential in the $G_{\rho T}(q,t)$ may not be considered *per se* a way to introduce the mode-coupling theory in the hydrodynamic response [15].

IV. EXPERIMENTAL PROCEDURES

A. Laser system and optical setup

The lasers and the optical setup used to realize the HD-TG experiment are reported in Fig. 1. The pump infrared pulses at 1064 nm wavelength, are produced by a mode-locked Nd-YAG laser (Antares-Coherent) and then they are amplified by a regenerative Nd-YAG cavity (R3800-Spectra Physics) to reach 1 mJ at 1 kHZ of repetition rate with 100 ps of duration. The probing beam, at 532 nm wavelength, is produced by a diode-pumped intracavity-doubled Nd-YVO (Verdi-Coherent); this is a CW single-mode laser characterized by an excellent intensity stability with low and flat noise-intensity spectrum. The beam intensities and polarizations are controlled by two couples of half-wave plate and polarizer.

The optical setup, shown in Fig. 1, uses a phase grating as a diffractive optical element (DOE): controlling the depth of the grooves and their spacing, it is possible to obtain very high-diffraction efficiency, better than 80% on the first two orders. Since we have to diffract both 1064 and 532 nm, a compromise must be used. The chosen DOE (made by Edinburgh Microoptics) gives on a single beam at first order a 12% diffraction efficiency for the 532 nm and 38% for the 1064 nm. Different spacings may be used to change the q vector. With the aid of a dichroic mirror (DM), the excitation and probing beams are sent collinearly on the DOE that produces the two excitation pulses (E_{ex}), the probing (E_{pr}), and the reference beam (E_l). These beams are collected by a first achromatic lens (AL1), cleaned by a spatial mask to block other diffracted orders and then recombined and focused by a second lens (AL2) on the sample. The local laser field is also attenuated by a neutral density filter and adjusted in phase passing through a couple of quartz slabs properly etched. The excitation grating produced on the sample is the mirror image of the enlightened DOE phase pattern. If AL1 and AL2 have the same focal length, the excitation grating has half the spacing of DOE [9]. This type of setup automatically gives the Bragg condition on all the beams and it produces a very stable phase locking between the probing and reference beam, a crucial parameter to realize a heterodyne detection. To properly test the acoustic damping [7], the excitation beam is focalized by a cylindrical lens (CL2) on the DOE and so the produced grating on the sample is extended in the q direction (about 5 mm); vice versa, the probing beam is focalized in a circular spot (0.5 mm) on the sample, through the two lens CL1 and CL2. We reduced the laser energy on the sample to the possible lowest level to avoid undesirable thermal effects, and the CW beams have been gated in a window of about 1 ms every 10 ms by using a mechanical chopper synchronized with the excitation pulses. The mean exciting energy was 7 mW (35 μJ per pulse at 100 Hz) and the probing energy was 6 mW. The reference beam intensity is very low and it is experimentally adjusted, using a variable neutral filter, to be about 100 times the intensity of the diffracted signal. With these intensities, the experiment is deeply inside the linear-response regime and no dependence of HD-TG signal shape on the intensities of the beams can be detected. The HD-TG signal, after it has been optically filtered, is measured by the a fast avalanche photodiode (APD) with a bandwidth of 1 GHz (Hamamatsu), amplified, and recorded by a digital oscilloscope with 1 GHz-4 Gs (LeCroy).

The OTP, from Fluka (99%), has been purified by repeated crystallization in methanol and dried under vacuum. The sample is kept in an aluminum cell with a teflon coating and it shows a stable supercooled phase. The cell temperature is controlled by a cryostat system (helium closed circle, Cryogenics) with a platinum resistance dipped in the sample.

B. Data collection and handling

The OTP measured signal spans over many decades in time, typically up to about 1 ms, so we recorded the data in a pseudologarithmic time scale. We use a fast time window

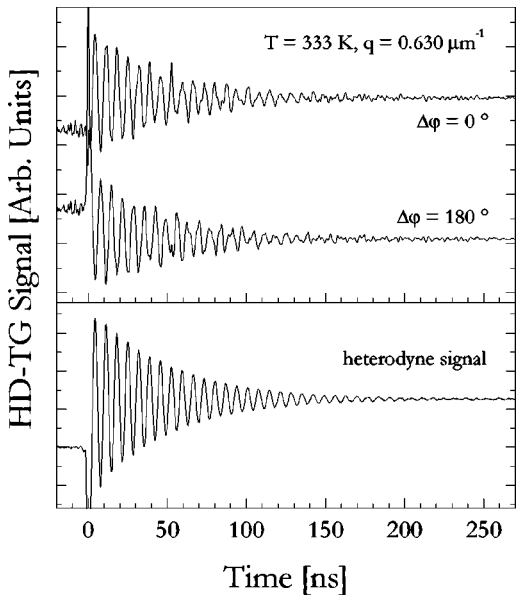

FIG. 2. Typical HD-TG raw data corresponding to phase difference between signal and local reference of $\Delta\varphi=0°$ and $\Delta\varphi=180°$ (above); pure HD-TG signal (below) is obtained by substracting the two previous signals. The subtraction permits to improve substantially the signal/noise ratio, to remove the homodyne and all spurious contributions that are phase independent.

($0-1\,\mu$s range with a 250 ps time step), an intermediate ($0-20$ μs range with a 10 ns time step), and a long one ($0-1$ ms range with a 200 ns time step) and then the measurements are merged in a single data file, without any problems of overlapping. Each data is an average of 5000 recording (corresponding to about one minute of acquisition time) and this is enough to produce an excellent signal-to-noise ratio. In order to get rid of the homodyne and other spurious signals, we recorded two measurements at different phases of the local field, the first signal S_+, with $\Delta\varphi_+=2n\pi$ and a second one S_-, with $\Delta\varphi_-=2(n+1)\pi$ [see Eq. 2] and then we subtracted S_- from S_+ to extract the pure HD signal, S_{HD} [see Eq. 3]. From Fig. 2, where we have reported two typical S_+ and S_- signals and the extracted S_{HD}, it is clear how this procedure increases substantially the quality of data.

We measured the relaxation processes of OTP as a function of temperature for three different q values: $q=0.338$, 0.630, 1.000 $\mu\,\mathrm{m}^{-1}$. The wave vectors are evaluated by the geometry of the experiment and are affected by 0.8, 0.6, and 0.4 % error, respectively. For each wave vector, we take data as a function of temperature in a range, $243-373$ K, that largely covers the liquid and supercooled region around $T_c \sim 290$, being $T_g=244$ K and $T_m=329$ K. In Fig. 3, we show in linear-log scale some representative HD-TG data on glass-forming OTP. This figure shows clearly how the density dynamics of OTP is characterized by three main dynamical processes: an acoustic phonon, a structural relaxation that appears as a rise in the signal, and by the final thermal relaxation. The damping of acoustic phonon and the structural processes are strongly temperature dependent. There is a temperature range where these ''modes'' (acoustic phonon,

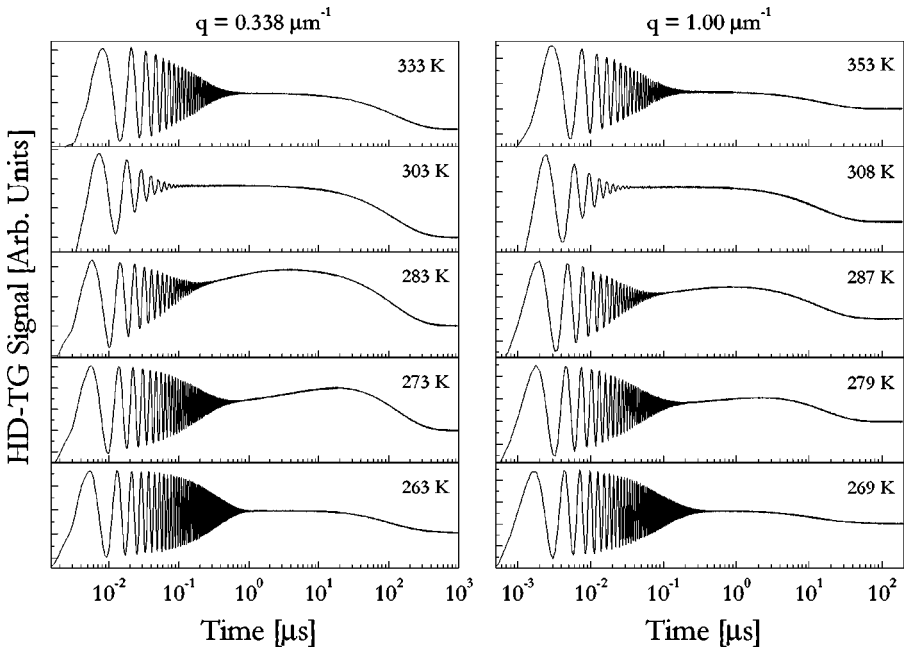

FIG. 3. HD-TG data on OTP for two wave vectors, $q=0.338$, and $q=1\ \mu\mathrm{m}^{-1}$, at several temperatures. The data, at all temperatures, show damped acoustic oscillations at short times and thermal diffusion at long times. Decreasing of temperature of the structural relaxation mode, typical of complex liquids, appears at first as a strong acoustic damping ($\omega_A\tau_S\sim 1$ condition) and later as gradual rise of TG signal.

structural, and thermal relaxation) are characterized by separated time scales. Some physical quantities, such as the sound velocity, may be directly obtained from HD-TG, data but a complete analysis of them requires a fitting procedure.

We tested the response function defined in Eqs. (7), (11) performing a nonlinear least-square fit on our OTP data. The fitting includes a convolution with the instrumental response (APD, amplifier, and oscilloscope); this convolution procedure is particularly important at short times of the signal, where the acoustic oscillations take place. We found this response function able to reproduce our HD-TG data on a large-time windows but not on the whole measured time scale, See Fig. 4. Indeed, the very fast time scale (0 -2 ns) is fairly reproduced, even if an extreme care has been taken to include all the possible signal contributions, e.g., the instantaneous signal due to the molecular hyperpolarizzability. Actually, it is not surprising that an hydrodynamics approach is not appropriate on a fast-time scale since it does not take into account any molecular proprieties. Again, as we will discuss later in detailed see Sec. V, we found that in the long time scale ($0.1-1$ ms) and in the intermediate temperature range, this response function is not able to reproduce completely our data. In fact, they show a relaxation pattern that may never be explained by the used response function, see Fig. 9. From our fit on OTP, it is clear the presence of both the excitation mechanisms: the electrostrictive effects (ISBS contribution) and the thermal effects (ISTS). We may estimate about 60% of ISBS against 40% of ISTS for $q=0.338\ \mu\mathrm{m}^{-1}$ and this ratio increases when the value of the wave vector increases. Nevertheless, the two contributions may be safely disentangled from the fits, thanks to the linear access to the response function. To evaluate the errors for such complex data and fitting function is not a trivial task, we used an ''*a posteriori*'' procedure. We repeated the experiment, getting for each temperature and wave vector several HD-TG signals, then we fit all the signals producing a distribution of parameters.

V. RESULTS

We used the previously defined response function [see Eqs. (5), (7), (11)] to extract the information about OTP dynamics from HD-TG data. The fitting parameters are: the acoustic frequency and damping rate (ω_A and Γ_A), the structural relaxation time and stretching parameter (τ_S and β), the thermal relaxation-time (τ_H), and the amplitude constants (A, B, and C). In Fig. 5 we report the sound velocity, $c_A=\omega_A/q$, and the damping rate Γ_A, see also Table I. These two parameters are extracted with very small uncertainties, less then 1%, for all the investigated temperatures and wave

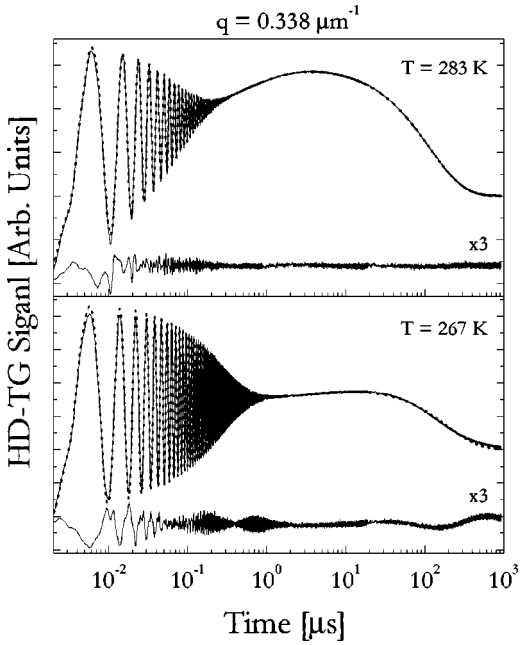

FIG. 4. HD-TG data (solid lines), fits (dotted lines) and residues $x3$ (lower lines) for OTP, at the two temperatures, $T=288$ K and $T=267$ K at wave-vector $q=0.338\ \mu\mathrm{m}^{-1}$.

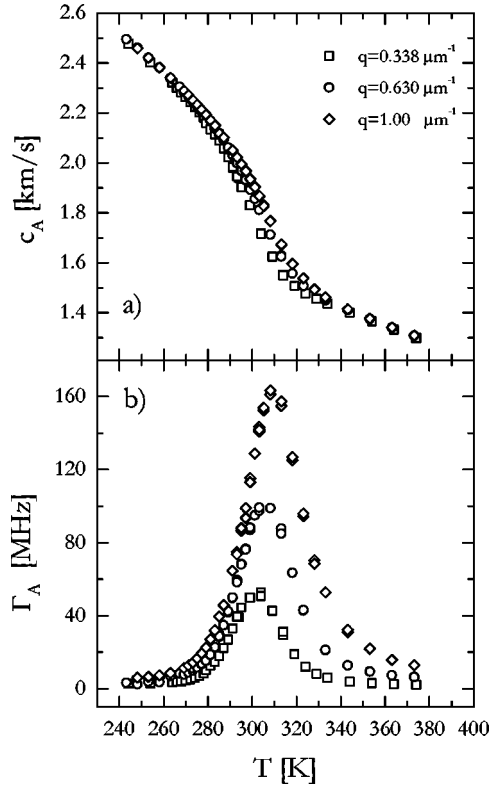

FIG. 5. Sound velocities c_A (a) and acoustic damping rates Γ_A (b) versus temperature from fits of HD-TG data at the investigated wave vectors. At each q value, the sound dispersion and damping rate reach the maximum at the temperature for which $\omega_A \tau_S \sim 1$.

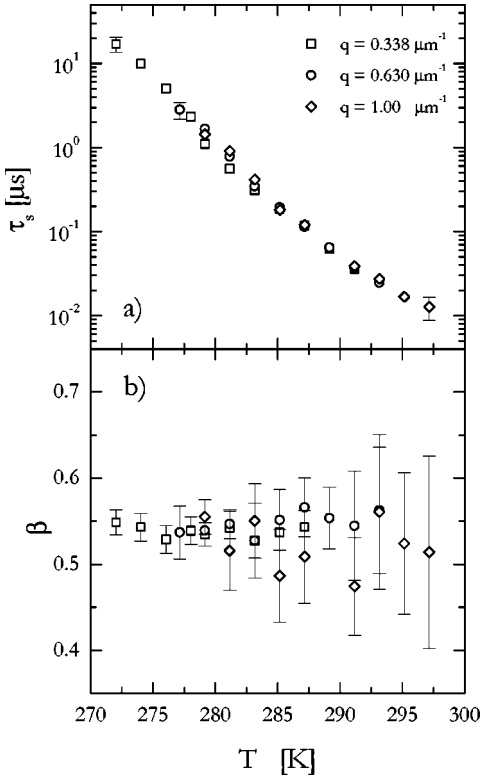

FIG. 6. Structural relaxation times τ_S and stretching parameter β versus temperature at the three wave vectors analyzed.

vectors. The sound velocity, see Fig. 5(a), shows the typical temperature dependence of viscoelastic liquids. The velocity increases lowering the temperature and shifts from two linear-dependence regimes, at high temperatures, the velocity almost corresponds to the adiabatic sound velocity c_0, while at low temperatures, it corresponds to the solidlike or ''infinite'' frequency sound velocity c_∞. In the transition region, starting from few tens of degrees above T_c, there is a rapid increase of c_A toward c_∞. At higher wave vector, the shift between the two regime appears at higher temperature. This behavior reflects the rapid variation of the structural relaxation time with the temperature. In fact, at high temperatures, the structural relaxation times are shorter than the phonon oscillation period, $\tau_S \ll (\omega_A)^{-1}$, therefore, the acoustic phonon is weakly coupled with the structural processes and it shows a soft damping. Again, at low temperatures, when $\tau_S \gg (\omega_A)^{-1}$, the two processes are decoupled yielding again a soft damping of the sound waves. Vice versa, when $\tau_S \omega_A \sim 1$, the structural and acoustic phenomena have the maximum coupling and this produces a maximum in the damping rate, see Fig. 5(b). In the hypothesis of a single relaxation time, we can extract its value from the damping maximum, i.e., $\tau_S \sim (\omega_A)^{-1}$. We found: $\tau_S \sim 0.6$ nsec for $q = 1\ \mu\mathrm{m}^{-1}$, $\tau_S \sim 0.9$ nsec for $q = 0.63\ \mu\mathrm{m}^{-1}$ and $\tau_S \sim 1.6$ nsec for $q = 0.338\ \mu\mathrm{m}^{-1}$.

When the temperature is around T_c, the structural relaxation process is appearing in the HD-TG pattern as a bump after the vanishing of the acoustic oscillations, see Fig. 3. In this case, the structural times may be easily extracted from the fitting procedure with confidence. Indeed, it has been possible to get reliable structural parameters τ_S and β only in a q-dependent restricted range of temperature, namely, in the range $T = 279-297$ K for $q = 1\ \mu\mathrm{m}^{-1}$, $T = 277-293$ K for $q = 0.63\ \mu\mathrm{m}^{-1}$, and $T = 272-287$ K for $q = 0.338\ \mu\mathrm{m}^{-1}$. This fact reflects the limitation of the fitting formulas, [Eqs. (7), (11)], since they fully apply only when a time scale separation exists among the various characteristic times, as already pointed out. Nevertheless, the safely extracted structural parameters are covering a key temperature range for OTP around the its critical temperature. The OTP structural parameters are reported in Fig. 6. They are covering three decades in time that were not previously investigated, from about 10 nsec up to 20 μsec, and they are indeed quite difficult to be reached by other techniques, both in (q,t) and (q,ω) space. Within the uncertainties, resulting essentially from the fitting procedure, the structural relaxation times do not show any q dependence and in the stretching parameter, we cannot recognize any temperature dependent, too. We want to remark that the stretching parameter is really affected by large uncertainties, see Fig. 6(b). Unfortunately, also another relevant quantity, i.e., the nonergodicity parameter $f_{q\to 0}$, which can be estimated from Eq. (10), is affected by large uncertainties. Within them, the $f_{q\to 0}$ parameter of OTP from our HD-TG data does not show the cusplike behavior predicted by the mode-coupling theory [15], as is evident from Fig. 7. On the other hand, the behavior of the nonergodicity parameter has been measured by neutron scattering for different high values of wave vector

TABLE I. Sound frequencies and damping rates with their relative errors for the analyzed q values in the range 243 – 374 K. To avoid an overcrowded table, we report only some temperatures.

	$q=0.338$ μm^{-1}		$q=0.630$ μm^{-1}		$q=1.00$ μm^{-1}			
T (K)	ω_A (GHz)	Γ_A (MHz)	ω_A (GHz)	Γ_A (MHz)	ω_A (GHz)	Γ_A (MHz)	$\Delta\omega_A/\omega_A$	$\Delta\Gamma_A/\Gamma_A$
243.2			1.572	3.30			$\leqslant 0.1\%$	$\leqslant 1\%$
244	0.8348	2.94					”	”
253.2			1.525	3.81	2.423	6.47	”	”
254	0.8094	3.02					”	”
263.2			1.474	6.90	2.343	8.57	”	”
264	0.7821	3.52					”	”
270	0.7629	4.53					”	”
271.2			1.424	8.90	2.273	12.7	”	”
279.2	0.7275	10.1	1.381	15.2	2.195	22.3	”	”
287.2	0.693	22.1	1.319	35	2.10	45	$\leqslant 0.5\%$	$\leqslant 5\%$
295.2	0.642	44	1.240	68	2.00	86	”	”
303.2			1.139	93	1.868	142	”	”
304	0.577	50					”	”
313.2			1.025	86	1.674	156	”	”
314	0.52283	30					”	”
323.2			0.948	41	1.539	95	$\leqslant 0.1\%$	$\leqslant 1\%$
324	0.4977	11.9					”	”
333.2			0.913	20.8	1.462	52.7	”	”
334	0.4837	5.96					”	”
343.2			0.888	12.8	1.415	31.5	”	”
344	0.4715	3.87					”	”
353.2			0.866	9.37	1.377	21.8	”	”
354	0.4600	2.93					”	”
363.2			0.8441	7.34	1.342	15.8	”	”
364	0.4485	2.47					”	”
373.2			0.8236	6.38	1.309	12.8	”	”
374	0.4375	2.23					”	”

and according to an extrapolation of its slope in the limit $q \rightarrow 0$, the cusplike shape seems to be hardly visible [16].

The fitting parameter τ_H, the thermal relaxation time, defines the final decay of the HD-TG signal and it is safely extracted when the condition $\tau_H \gg \tau_S$ is verified. Since $\tau_H \sim 100$ μsec and it is typically not strongly temperature dependent until Tg [7], it should be safely extracted in the range from 373 K down to 270 K. In Fig. 8, we report the thermal diffusivity, $\chi=(\tau_H q^2)^{-1}=k(\rho_o C_p)^{-1}$, resulting from the investigated three wave vectors in the whole temperature range. In the high-temperature range, χ shows the expected smooth variation and the independence of q. Approaching the critical temperature, a strong deviation is showing up: starting from about 275 K at $q=0.338$ μm^{-1} (and from temperatures even higher at higher q) an anomalous strong decrease in the thermal diffusivity is coming from our fit. The decrease is so strong that the longer decay is clearly visible in a semilogarithmic plot of the data, see Fig. 9. This effect could be an interaction between the structural and thermal relaxation-times τ_S and τ_H, that are getting closer decreasing the temperature. However when the thermal diffusivity starts deviating, the structural and thermal relaxation times seem to be too far each other, e.g., at $q=0.338$ μm^{-1} the deviation start at about $T=275$ K, where $\tau_S=15$ μs and $\tau_H=115$ μs. Nevertheless, we must remember that τ_S is a relaxation-time representative of a large distribution of times.

Further, in the region of the thermal diffusivity dip, the HD-TG data show a second very slow decay: indeed, it is clear from Fig. 9, that the slow relaxation at $T=283$ and 253 K are characterized by a single exponential relaxation, the thermal decay, and vice versa at 267 K some other relaxation is appearing. It is fairly obvious that the used response function [Eqs. (7), (11)] is not able at all to reproduce these features. As regards the subsequent large increase of the thermal diffusivity at low temperature where the structural relaxation times are found even longer than the thermal relaxation, the experiments of specific heat spectroscopy on glass formers [17] suggest that this increase may be due to C_p variations, approaching the solidlike or high-frequency response.

VI. DISCUSSION AND CONCLUSIONS

The present analysis of the HD-TG data of glass-forming OTP, around its critical temperature, in terms of density hy-

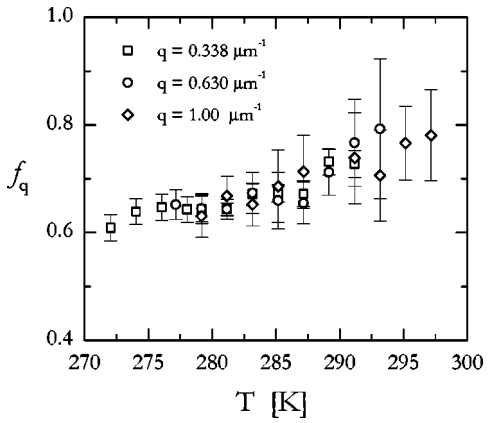

FIG. 7. Temperature dependence of the Debye-Waller factor $f_{q\to 0}(T)$ in OTP, obtained by fits, at all wave vectors. There is no evidence of a mode-coupling theory (MCT) cusp in the analyzed temperature range.

drodynamics response shows some clear results but it also opens some problems in the data interpretation. To get a further understanding, we compare our parameters with the other literature data. In Fig. 10, we report our sound velocities together with the data from Brilluoin light scattering (LS) [18] and ultrasound experiments [19]. Here, the agreement is very nice. As we expected, there is a clear dispersion effect in q, as the LS data are taken at much higher wave vectors, and the extreme values c_0 and c_∞ are approached at high and low temperatures, respectively. It is evident that the HD-TG experiment is able to measure the sound velocity at wave vectors in an otherwise difficult range, too low for LS techniques but too high for ultrasound experiments. In fact, in our experiment, ω_A ranges from 0.4 to 2 GHz with $\Gamma_A \sim 2-160$ MHz.

Our structural relaxation times are compared with the light scattering (LS) [20,21], photon correlation (PC) [20,22] and time-resolved optical Kerr effect (OKE) data [23]. All these data are extracted from experiments performed with depolarized light geometry and so the influence of the orientational dynamics can be non negligible. Nevertheless, our

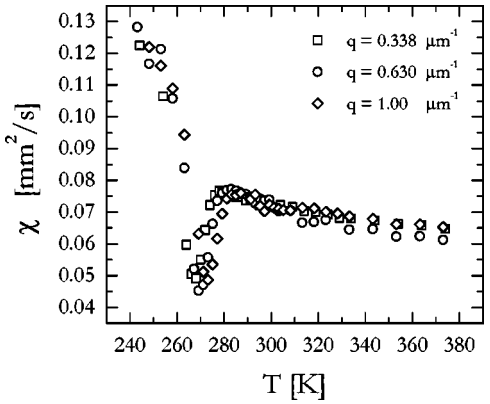

FIG. 8. Thermal diffusivity versus temperature. For every investigated q value, the extracted thermal diffusivity show, at low temperatures, a peculiar behavior not in agreement with the temperature dependence of the thermodynamic thermal diffusivity.

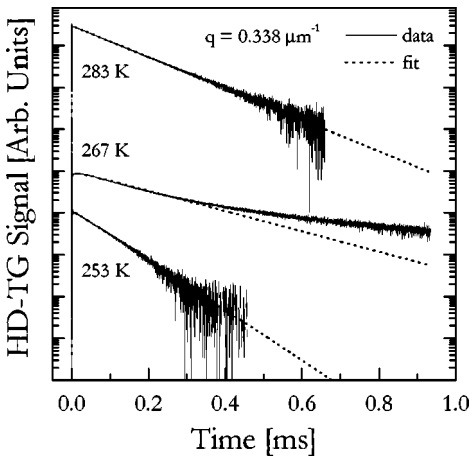

FIG. 9. HD-TG data (solid curves) and fits (dotted curves), at wave-vector $q=0.338\ \mu\mathrm{m}^{-1}$ at some temperatures, are plotted in log-lin scale to show the complex decay at long times. In the intermediate temperatures range, where the thermal diffusivity (Fig. 8) shows the anomalous dip, the used fitting function (11), is not able to reproduce the decay at long times.

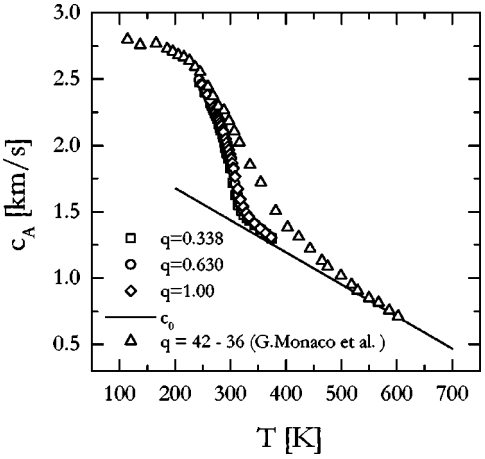

FIG. 10. OTP sound velocities from HD-TG data, LS data [18], and ultrasonic measurements [19].

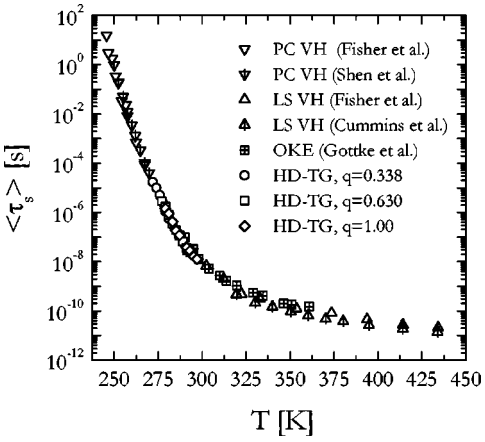

FIG. 11. OTP structural relaxation times from HD-TG data, LS [20,21], PC [20,22], and OKE data [23].

OTP data, spanning from 10^{-8} up to 10^{-5} sec, nicely cover the gap present between LS, OKE, and PC measurements and they follow the same course, as we can see in Fig. 11. This good agreement has some implication in OTP dynamics, suggesting that the orientational and translational dynamics, have substantially the same temperature dependence, in the investigated temperature range, with very similar relaxation times.

The cusplike behavior of the Debye-Waller factor, expected in the frame of mode-coupling theory for a fragile glass such as OTP, is not recognizable.

We would like to stress that the slow thermal decay, at relatively low temperature, did not show a simple single exponential decay and it cannot be properly characterized by the simple hydrodynamics model used in this paper. We have found this behavior common to other several glass formers: glycerol, *m*-toluidine, salol [24]. In our opinion, the apparent modification of the thermal diffusivity has to be addressed to effects of the structural dynamics on the thermalization process. In other words, the heat flux, produced by the weak absorption of the pump-laser pulses, modifies the kinetic energy of the different degree of freedom and not all of them thermalize in a very short-time scale. Furthermore, part of the roto-translational energy thermalizes through collective rearragements that acts on the structural time scale. This kind of process is also responsible for the frequency dependence of the specific heat. A more suitable hydrodynamic treatment for the heat transport should be able to take into account the complex relaxation patterns found in the present experiment.

ACKNOWLEDGMENTS

We thank F. Barocchi, K. A. Nelson, R. M. Pick, and G. Ruocco for very helpful suggestions and discussions. This work was supported by the Commission of the European Communities through Contract No. HPRI-CT1999-00111, by MURST and by INFM through Project No. TREB-Sez.C-PAISS1999.

[1] J. Wong and C. A. Angell, *Glass Structure by Spectroscopy* (Marcel Dekker Inc., New York, 1976); P. G. Debenedetti, *Metastable Liquids* (American Chemical Society, Washington, 1996); J. T. Fourkas, D. Kivelson, U. Mohanty, and K. A. Nelson, *Supercooled Liquids* (Princeton University Press, Princeton, NJ, 1996).

[2] W. Götze, J. Phys.: Condens. Matter **11**, A1 (1999); H.Z. Cummins, *ibid.* **11**, A95 (1999).

[3] R. Torre, P. Bartolini, R.M. Pick, Phys. Rev. E **57**, 1912 (1998); R. Torre, P. Bartolini, M. Ricci, R.M. Pick, Europhys. Lett. **52**, 324 (2000); G. Hinze, D.D. Brace, S.D. Gottke, and M.D. Fayer, Phys. Rev. Lett. **84**, 2437 (2000).

[4] A. Taschin, R. Torre, M. Ricci, M. Sampoli, C. Dreyfus, and R. Pick, Europhys. Lett. **56**, 407 (2001).

[5] G. Hinze, R.S. Francis, and M.D. Fayer, J. Chem. Phys. **88**, 6477 (1999).

[6] H. J. Eichler, P. Gunter, and D. W. Pohl, *Laser-Induced Dynamic Gratings* (Spriger-Verlag, Berlin, 1986).

[7] Y. Yang and K.A. Nelson, Phys. Rev. Lett. **74**, 4883 (1995), Y. Yang and K.A. Nelson, J. Chem. Phys. **103**, 7732 (1995); D.M. Paolucci and K.A. Nelson, *ibid.* **112**, 6725 (2000).

[8] Y. Yan and K.A. Nelson, J. Chem. Phys. **87**, 6240 (1987); **87**, 6257 (1987).

[9] A.A. Maznev, K.A. Nelson, and J.A. Rogers, Opt. Lett. **23**, 1319 (1998).

[10] G.D. Goodno, G. Dadusc, and R.J. Dwayne Miller, J. Opt. Soc. Am. B **15**, 1791 (1998).

[11] B. B. Berne and R. Pecora, *Dynamic Light Scattering* (Wiley, New York, 1976).

[12] J. P. Boon and S. Yip, *Molecular Hydrodynamics* (McGraw-Hill, New York, 1980).

[13] Y. Yang and K.A. Nelson, J. Chem. Phys. **103**, 7722 (1995).

[14] According to the hydrodynamics model [7], the whole ISBS signal is the following:

$$G_{\rho\rho}(q,t) \simeq C[e^{-\Gamma_A t}\sin(\omega_A t)] + D[-e^{-\Gamma_A t}\cos(\omega_A t) + e^{-(t/\tau_S)^{\beta}}].$$

Indeed, the amplitude D has been found in the previous work to be negligible. Also, in the present paper, we found the D terms to be very small and not affecting at all the fitting results. Nevertheless, since this test is based only on the fitting procedure a final conclusion cannot be given about the intensity of structural contribution in the ISBS signal.

[15] W. Götze and L. Sjögren, Rep. Prog. Phys. **55**, 241 (1992).

[16] A. Tölle, H. Schober, J. Wuttke, and F. Fujara, Phys. Rev. E **56**, 809 (1997); E. Bartsch, F. Fujara, B. Geil, M. Kiebel, W. Petry, W. Schnauss, H. Sillescu, and J. Wuttke, Physica A **201**, 223 (1993).

[17] N.O. Birge, Phys. Rev. B **34**, 1631 (1986).

[18] G. Monaco, D. Fioretto, L. Comez, and G. Ruocco, Phys. Rev. E **63**, 61502 (2001).

[19] G. D'Arrigo, J. Chem. Phys. **63**, 61 (1975).

[20] W. Steffen, A. Patkowski, G. Meier, and E.W. Fisher, J. Chem. Phys. **96**, 4171 (1992); W. Steffen, A. Patkowski, H. Glaser, G. Meier, and E.W. Fisher, Phys. Rev. E **49**, 2992 (1994); A. Patkowski, E.W. Fisher, W. Steffen, H. Glaser, M. Baumann, T. Ruths, and G. Meier, *ibid.* **63**, 61503 (2001).

[21] H.Z. Cummins, G. Li, W. Du, Y.H. Hwang, and G.Q. Shen, Prog. Theor. Phys. Suppl. **126**, 21 (1997).

[22] Y.H. Hwang and G.Q. Shen, J. Phys. C **11**, 1453 (1999).

[23] S.D. Gottke, D.D. Brace, G. Hinze, and M.D. Fayer, J. Phys. Chem. B **105**, 238 (2001).

[24] M. Sampoli *et al.* (unpublished); R. DiLeonardo *et al.* (upublished).